# Nonlinear Parameter and State Estimation Approach in End-stage Kidney Disease Patients

Rammah M Abohtyra, Tyrone L Vincent

***Abstract*—*Objective:* There are nearly 786,000 Americans with end-stage Kidney disease (ESKD), of which 71% rely on life-saving hemodialysis (HD) treatment. HD care costs Medicare annually in excess of $70 billion. One primary goal of HD treatment is to remove excess fluid via ultrafiltration. Intradialytic hypotension (IDH), a significant reduction in blood volume due to an imbalance between ultrafiltration and interstitial to intravascular fluid refilling rates, has severe implications for morbidity and mortality. However, fluid and blood volume are not accessible. It has been suggested that knowledge of extracellular fluid and absolute blood volume should improve HD outcomes. *Methods:* The new estimation approach combines a validated physiological-based fluid volume model during ultrafiltration, the nonlinear least squares method with an uncertainty quantification technique, and the unscented Kalman filter. *Results:* We develop a novel estimation approach that estimates the underlying model parameters, bounds error estimation due to model uncertainty and measurement noise, reconstructs unmeasured fluid and blood volume, and predicts personalized outcomes (hematocrit), during HD treatment. Finally, we test the performance of our approach using actual HD data. *Conclusion:* The extracellular (plasma, interstitial) fluid volume, absolute blood volume, and fluid shift/refill parameters can be estimated and bounded by the Fisher information matrix lower bounds. In addition, fluid volume corrections and personalized predictions for the blood volume evolution can be achieved during ultrafiltration by fitting the underlying parameters to a patient's data. *Significance:* This novel estimation algorithm, readily available for integration in current HD machines, could improve HD treatment outcomes.**

***Index Terms*—Nonlinear estimation, Hemodialysis, ultrafiltration, hematocrit (HCT), absolute blood volume, and UKF.**

## I. Introduction

MORE than 37 million Americans have kidney disease. Among them, nearly 786,000 live with end-stage Kidney disease (ESKD), of which 71% rely on hemodialysis (HD) treatment [1]. HD care is a life-saving treatment, with a Medicare annual cost of over $70 billion [1]. Patients in ESKD are often suffering from multiple acid-base derangements and fluid shift complications. During HD treatment fluid accumulation is removed by ultrafiltration and acid-base derangement is corrected [2]–[4]. Most patients with ESKD are treated with 3-4 HD sessions per week, and each session is 3-5hrs long, but standard HD therapy does not guarantee optimal outcomes for those individuals [5]. Too high or too low removal rate, or 'ultrafiltration rate' (UFR), during the HD treatment is associated with increased morbidity and mortality risk [6]–[8], with a 15-20% mortality rate under the first year of HD maintenance [9].

The standard ultrafiltration protocol applies high constant rates, generating an imbalance between fluid removal and interstitial to intravascular fluid refilling rates that causes a significant reduction in the absolute blood volume, especially at the end of HD therapy when the fluid refilling rate is low. This imbalance provokes intradialytic hypotension (IDH), (intradialytic systolic blood pressure (SBP) < 90 mmHg) in 25-60% of HD treatments, and is associated with a higher risk of cardiovascular morbidity and rate of death (20-25% death rate each year under HD maintenance therapy) [10].

Conversely, an inadequate UFR during HD may lead to Hypervolemia (fluid overload). Fluid overload is associated with adverse outcomes, including hypertension, left ventricular hypertrophy, and cardiac mortality [11], [12]. Both IDH and fluid overload are serious complications of fluid management during HD therapy and are associated with increased cardiovascular morbidity and mortality.

It has been recommended that to improve HD patient's outcomes, personalized UFR protocols, which are tailored to patient's physiology and provide patient-specific UFR to minimize IDH risk while avoiding fluid overload, are needed [13]–[15]. These protocols generally control the ultrafiltration by decreasing the removal rate towards the end of the HD session, which induces an adequate balance between ultrafiltration and vascular refilling, defined as a fluid shift from the interstitial compartment into the intravascular compartment to overcome the reduction in the circulating blood volume [16], [17].

The interstitial fluid (fluid between the cells) and intravascular fluid are the main components of the extracellular fluid compartment in the body. The intravascular fluid contains blood, consisting of plasma and red blood cells. The fluid exchange (shift/refill) between the intravascular and interstitial compartments is governed by the Starling forces, including hydrostatic and osmotic pressure gradient across the capillary membrane, capillary permeability, and overall fluid volume status of individuals [18], [19]. During HD treatment, ultrafiltration removes plasma while keeping red blood cell mass fixed [20].

It is not possible to measure the absolute blood volume during HD. Instead, in an HD setting, the relative blood volume (RBV) is estimated based on changes in specific blood components, such as hematocrit (HCT using Crit-line monitor), hemoglobin (HGB), or total blood protein concentration (TBP). The HCT can be estimated from non-invasive measurements of optical integrated into the dialysis machine [21]. Methods based on radio-isotope dilution have been developed to measure the blood volume, but these methods are not easily applied on a regular basis [22].

Since direct observation of fluid refilling rate during HD therapy is not accessible, estimation of fluid refilling rates is required [23]. Several clinical studies have been conducted

to estimate fluid refilling rate during HD [24], [25], using specific UFR protocols. For example, in [24], to prevent IDH, a UFR protocol with two phases was applied to determine the amount and direction of body fluid compartment with two objectives 1) maintain blood volume at a baseline followed by an increase in UFR to exceed the refilling rate, and 2) raise the blood volume toward the baseline by decreasing UFR, which sometimes requires turning the UFR to zero. Consequently, the UFR protocol may lead to fluid overload or extend the time of the HD session.

The prediction of fluid volume in HD patients remains one of the most challenging diagnostic problems clinicians face daily [26], [27]. Determining the amount of excess fluid volume by targeting the patient's dry weight is a significant part of HD. Dry weight, a minimum weight for a patient to leave HD treatment without symptoms or signs such as edema and IDH, is estimated only by the clinicians [19]. Correctly estimating the dry weight minimizes the risk to the cardiovascular system and decreases the mortality rate [28]. However, failures in this prediction may lead to inappropriate therapy, and potentially more severe outcomes [11]. Several methods, including atrial or brain natriuretic peptide levels, ultrasound, and blood pressure, have been used to estimate fluid volume [29], [30]; however, some of which are not accurate [30]. Recently, a machine learning method has been used to predict dry weight for dialysis patients [31]; but this method does not provide physiological insights into the fluid shift/refill mechanisms.

Therefore, we propose a nonlinear parameter and state estimation approach for ESKD patients. Our approach offers the potential to overcome these limitations and provides fidelity by using a validated physiological-based mathematical model with interpretable parameters and gives physiological insights into fluid volume management during HD treatment.

The main contribution of this paper is the development of a nonlinear model-based estimation approach that (1) estimates the initial extracellular (plasma and interstitial) fluid volume, initial absolute blood volume, and a set of fluid shift/refill parameters, with parameter estimation error bounded by the Fisher information matrix, and (2) updates the unobservable fluid and blood volume and predicts the evolution of blood volume during ultrafiltration. We examine the performance of this method using clinical data, which comprises 'typical' UFR profiles used frequently in the HD centers.

The paper is organized as follows. Section II summarizes the nonlinear, two-compartment model describing the extracellular fluid volume dynamics during HD treatment. Section III presents the results, including the parameter estimation approach and estimation sensitivity analysis. Section IV illustrates the implementation of our algorithm using clinical HD data examples. Section V provides discussion and future directions, and conclusions are made in Section VI.

## II. Materials and Methods

The estimation approach utilizes a validated two-compartment fluid volume model defined by nonlinear continuous-time differential equations and used for patients in ESKD. Previously, we have successfully used the linearized version of this model to develop a personalized UFR method [13], [14], but here we use the 'full' nonlinear model.

### A. Two Compartment Fluid Volume Model

Briefly, we provide a summary about the nonlinear two-compartment model illustrated in Fig. 1. The model captures the extracellular fluid volume (EFV) dynamics, which comprises of the intravascular (plasma) and interstitial compartments, separated by a capillary membrane. The model includes the lymphatic flow, which returns a portion of fluid from the interstitial space into the intravascular space.

The states are the plasma volume, $V_p$ (L), and the interstitial fluid volume, $V_i$ (L); while the input, $u$, is the ultrafiltration rates (UFRs) (L/min).

The output is the hematocrit (HCT), which is the proportion of the total absolute blood volume ($V_{rbc} + V_p$) that consists of red blood cells (RBCs) volume, $V_{rbc}$ (L), i.e., $HCT = V_{rbc}/(V_{rbc} + V_p)$, which is usually expressed as a percentage in clinical practices but is expressed here as a fraction.

The microvascular flow, $Q_f$ (refilling/filtration), describes the fluid exchange between the intravascular and interstitial spaces through the capillary membrane. The mathematical

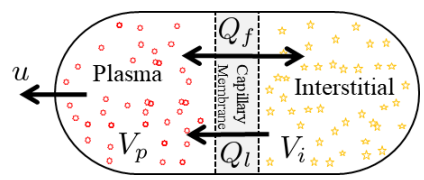


Figure 1. The two-compartment model consists of interstitial fluid volume ($V_i$) and intravascular (plasma) fluid volume ($V_p$) separated by a capillary membrane; microvascular flow ($Q_f$), lymph flow ($Q_l$), and ultrafiltration ($u$).

description of this model during HD is given by the nonlinear differential system:

$$\dot{V}_p = -Q_f(V_p, V_i) + Q_l(V_i) - u \tag{1a}$$

$$\dot{V}_i = Q_f(V_p, V_i) - Q_l(V_i) \tag{1b}$$

$$HCT = \frac{V_{rbc}}{V_{rbc} + V_p} \tag{1c}$$

where $Q_f$ (L/min) represents the microvascular (shift/refill) filtration flow, in which, $K_f$ (L/min.mmHg) is the transcapillary permeability coefficient; and $Q_l$ (L/min) represents the lymphatic flow:

$$Q_f(V_p, V_i) = K_f(\delta_p - \delta_\pi) \tag{2a}$$

$$Q_l(V_i) = g\tanh(hP_i) + l \tag{2b}$$

where $\delta_p$ and $\delta_\pi$ represent the hydrostatic and osmotic pressure gradients, respectively:

$$\delta_p(t) = (P_c(t) - P_i(t)) \tag{3a}$$

$$\delta_\pi(t) = (\pi_p(t) - \pi_i(t)) \tag{3b}$$

where $P_c$, $P_i$, $\pi_p$, $\pi_i$ refer to the hydrostatic capillary pressure, interstitial pressure, plasma colloid osmotic pressure, and interstitial colloid osmotic pressure, respectively; and $g$, $h$, and $l$ are constants. The equations of these components, nominal parameters, and constants are provided in the Appendix.

### B. Patient Fluid Volume Variability

The variability in fluid volume depends on several factors, including fluid compartment sizes, fluid status (overload), fluid shift/refill between interstitial and intravascular spaces [18], and patient's characteristics. Here, we select six underlying parameters of model (1) as patient-specific parameters and then use our approach to infer them from patient's HD data.

For determining an appropriate dry weight, we estimate the initial extracellular fluid volume, including plasma and interstitial fluid volume $V_p(0)$, $V_i(0)$. We also estimate the absolute blood volume to predict IDH events during ultrafiltration. The initial absolute blood volume can be determined by estimating first $V_{rbc}(0)$ and then use $V_p(0)+V_{rbc}(0)$. Since ultrafiltration does not remove red blood cells [20], $V_{rbc}$ does not change. Therefore, the change in the absolute blood volume during ultrafiltration is due to changes in $V_p$.

The fluid refilling rate is regulated by the capillary filtration coefficient $K_f$, while hydrostatic capillary pressure parameters ($d_1$ and $d_2$) promote fluid movement from the intravascular space to interstitial space [18]. These parameters control fluid shift/refill across the capillary membrane wall, and they should be patient-dependent and estimated from HD data.

To reduce the number of unknown parameters, and since the lymphatic system returns a small amount of fluid to the intravascular space, and its parameters are insensitive to HCT, we assume the lymphatic flow parameters are fixed for all patients. Finally, we include these parameters in this vector $\theta = [V_p(0), V_i(0), V_{rbc}(0), K_f, d_1, d_2]^T$. The other parameters in Table II are nominal for all patients.

## III. Results

The estimation approach contains parameter and state estimation algorithms performed separately in sequence (See Fig. 2). The parameter estimation algorithm is based on the minimization method of nonlinear least squares introduced by Levenberg and Marquardt [32] to find parameters that provide the best fit between the nonlinear model and data. The estimated parameters is used, as an input, with the unscented Kalman filter (UKF) algorithm [33] to estimate multiple physiological variables of the nonlinear model (1) and quantify error estimation due to model uncertainty and measurement noise. The UKF fully reconstructs the unmeasured extracellular fluid volume (states) and absolute blood volume during ultrafiltration and predicts the model outcome (HCT) while correcting these variables based on given HCT measurements.

### A. Parameter Estimation Algorithm

The general form of our estimation approach utilizes a nonlinear model of continuous-time differential equation described by a state transition ($f$) and observation function ($h$), given in this form

$$\dot{x} = f(x, \theta, u, t),\ x(0) \neq 0 \tag{4a}$$

$$y = h(x, \theta, t) + v \tag{4b}$$

where $x \in \mathbb{R}^n$ denotes the unobserved state of the system; $u$ denotes the input to the system; and $\theta \in \mathbb{R}^p$ contains the model parameters whose values (or some of them) are estimated from data; $y$ is the model output; $t$ is the time $t_0 \leq t \leq t_f$ between initial, $t_0$, and final time, $t_f$; and $v$ represents measurement noise.

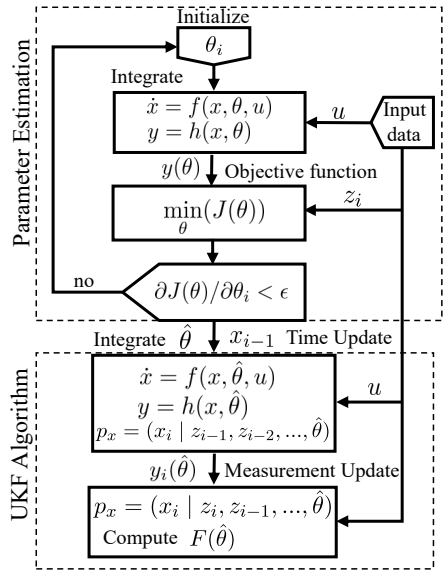


Figure 2. A schematic representation for Algorithm 1. The parameter estimation and UKF Algorithm are separately performed. The estimated parameter $\hat{\theta}$ is an input to the UKF Algorithm.

We solve for an optimal solution of $\theta$ using the least squares objective function:

$$J(\theta) = \min_\theta \sum_{i=0}^{N} (y_i(\theta) - z(t_i))^2 \tag{5}$$

where $z(t_i)$ refers to observed measurements, and $y_i(\theta)$ refers to the output of the nonlinear model (4), simulated for a given $\theta$. The solution of (5) is denoted by $\hat{\theta}$. Note that, as indicated in Fig. 2, the estimated parameter $\hat{\theta}$ is an input to the UKF Algorithm, and separately computed from the UKF.

### B. State Estimation and Prediction Algorithm

In order to estimate parameter uncertainty and make predictions of state trajectories, using the UKF, we introduce model uncertainty ($n$) into (4a) to come

$$\dot{x} = f(x, \hat{\theta}, u, t) + n \tag{6}$$

and made the assumption that the distribution of the model uncertainty ($n$) and measurement noise ($v$) in (4b) is piecewise constant over intervals of length $T_s$ seconds ($T_s$ is a sampling time), with the magnitude for interval $k$ ($k$ is an index) a Gaussian random vector with zero mean given by

$$n_k \sim \mathcal{N}(0, Q) \tag{7a}$$

$$v_k \sim \mathcal{N}(0, R) \tag{7b}$$

where $\mathcal{N}$ represents the notation for Normal Gaussian Distribution; $Q$ and $R$ are the covariance of model uncertainty and measurement noise, respectively. Consequently, we assume $x$ is Gaussian. Since $y$ is conditionally affected by the state $x$,

we also assume that $y$ is Gaussian. Thus, the conditional state and output density functions are Gaussian:

$$p_x(x_i \mid x_{i-1}, u_{i-1}, \hat{\theta}) = \mathcal{N}(x_i, Q) \tag{8a}$$

$$p_y(y_i \mid x_i, \hat{\theta}) = \mathcal{N}(h(x_i, \hat{\theta}), R) \tag{8b}$$

where $x_i$ is the solution to (4) with $n = 0$, initial condition $x_{i-1}$ and input $u_{i-1}$.

As illustrated in Fig. 2, the algorithm aims to find first $\hat{\theta}$ and then uses the UKF to compute the Fisher information matrix $F(\hat{\theta})$, update state, and predict output of model (4). Here, we provide iterative steps for updating the UKF, utilizing observations $z_0, z_1, \ldots, z_N$ at a sampling time $T_s$, and an input $u$, where $u$ is held as a piecewise constant during the interval $(i-1)T_s \leq t \leq iT_s$:

- $p_x(x_{i-1} \mid z_{i-1}, z_{i-2}, \ldots, \hat{\theta})$ represents the previous estimated state.
- $p_x(x_i \mid z_{i-1}, z_{i-2}, \ldots, \hat{\theta})$ represents the prediction update step (time update), obtained by integrating model (4) between time $t = (i-1)T_s$ to $t = iT_s$, with initial conditions $x((i-1)T_s) = E[x_{i-1} \mid z_{i-1}, z_{i-2}, \ldots, \hat{\theta}]$.
- $y(\hat{\theta}) = E[h(x_i, \hat{\theta}) \mid z_{i-1}, z_{i-2}, \ldots, \hat{\theta}]$ represents the prediction step of a measurement $z_i$.
- $p_x(x_i \mid z_i, z_{i-1}, z_{i-2}, ..., \hat{\theta})$ represents the measurement update step of the UKF.

Algorithm 1 below combines parameter estimation and state estimation and prediction (UKF) algorithms.

**Algorithm 1:** Parameter Estimation and Prediction

A. Parameter estimation algorithm
Initialize $\theta_i = \theta_0$, iterate for $i = 1, 2, \ldots$
**while** $\partial J(\theta_i)/\partial\theta_i > \epsilon$
  $i = i + 1$
  Numerically integrate $\dot{x} = f(\theta_i, u), y(\theta_i) = h(x, \theta_i)$
  Compute $e_i(\theta_i) = (y_i(\theta_i) - z(t_i))$ in $J(\theta_i)$ (5)
  Evaluate $\partial J(\theta_i)/\partial\theta_i < \epsilon$, If yes, then $\hat{\theta} = \theta_i$ **Stop**
**end while**
B. State estimation and prediction (UKF) algorithm
**for** $i = 1 : N$ **do (UKF**-Prediction)
  Numerically integrate $\dot{x} = f(\hat{\theta}, u), y(\hat{\theta}) = h(x, \hat{\theta})$ from time $t = (i-1)T_s$ to $t = iT_s$, with initial condition $x((i-1)T_s) = E[x_{i-1} \mid z_{i-1}, z_{i-2}, \ldots, \hat{\theta}]$.
  Update $p_x(x_i \mid z_{i-1}, z_{i-2}, \ldots, \hat{\theta})$ (Time update).
  Predict $z_i$ as $y(\hat{\theta}) = E[h(x_i, \hat{\theta}) \mid z_{i-1}, z_{i-2}, \ldots, \hat{\theta}]$
  Update $p_x(x_i \mid z_i, z_{i-1}, z_{i-2}, \ldots, \hat{\theta})$ (Meas. update).
**end for**
Compute $p_{z|\hat{\theta}}(z_i|\hat{\theta})$ and Fisher matrix $F(\hat{\theta})$.

### C. Parameter Estimation Sensitivity Analysis

We use the Fisher Information Matrix [34] to quantify the quality of the parameter estimation due to the model uncertainty and measurement noise. This analysis uses the following assumptions.

- The distribution of $y$ can we approximated by a Gaussian distribution.
- The experimental uncertainty is captured by model (4)
- The covariance of $y$ is independent of $\hat{\theta}$.
- The UKF is approximately optimal, so that the prediction errors are uncorrelated.
- The parameter estimates are unbiased

**Theorem 1.** *Under the assumptions listed above, the covariance of the parameter estimates ($P_\theta$) is bounded below by*

$$P_\theta \geq \left( \sum_{i=0}^{N-1} \frac{dy(\hat{\theta})^T}{d\hat{\theta}} S_i^{-1} \frac{dy(\hat{\theta})}{d\hat{\theta}} \right)^{-1} \tag{9}$$

*where $S_i$ is the covariance of the prediction error calculated using the UKF.*

**Proof:** For unbiased parameter estimates, the parameter estimate covariance is bounded below by the inverse of the Fisher information matrix (see e.g. [34]), which is calculated from the likelihood function. The likelihood function for the measurements $Z$ where $Z = [\ z_0 \quad \cdots \quad z_N\ ]^T$ is given by

$$p_{z|\hat{\theta}}(Z|\hat{\theta}) = \prod_{i=0}^{N-1} \frac{1}{(2\pi \mid S_i \mid)^{1/2}} \exp^{\left(-\frac{1}{2} e_i^T(\hat{\theta}) S_i^{-1} e_i(\hat{\theta})\right)} \tag{10}$$

where $e_i(\hat{\theta}) = (z_i - y_i(\hat{\theta}))$, in which $y_i(\hat{\theta})$ is the UKF one step ahead prediction; and $S_i = HP_iH^T + R$ is the covariance of the error $e_i(\hat{\theta})$, where $P_i$ is the estimated state error covariance at time $i$, and $H$ is the mapping from state to output (i.e., $H = [\ 1 \quad 0\ ]$ for the model (1)). Then the log-likelihood function is

$$\log p_{z|\hat{\theta}}(Z \mid \hat{\theta}) = -\frac{1}{2} \sum_{i=0}^{N-1} \log(2\pi \mid S_i \mid) - \frac{1}{2} \sum_{i=0}^{N-1} e_i^T(\hat{\theta}) S_i^{-1} e_i(\hat{\theta})$$

Then

$$\frac{d \log p_{z|\hat{\theta}}(Z|\hat{\theta})}{d\hat{\theta}} = \sum_{i=0}^{N-1} e_i^T(\hat{\theta}) S_i^{-1} \frac{dy_i(\hat{\theta})}{d\hat{\theta}}$$

The Fisher information matrix is given by the covariance of this expression, so we find

$$\begin{aligned} F =& E\left[ \left( \frac{d\log p_{z|\hat{\theta}}(Z|\hat{\theta})}{d\hat{\theta}} \right)^T \left( \frac{d\log p_{z|\hat{\theta}}(Z|\hat{\theta})}{d\hat{\theta}} \right) \right] \\ =& E\left[ \sum_{j=0}^{N-1} \sum_{i=0}^{N-1} \frac{dy_i(\hat{\theta})^T}{d\hat{\theta}} S_i^{-1} e_i^T(\hat{\theta}) e_i(\hat{\theta}) S_i^{-1} \frac{dy_i(\hat{\theta})}{d\hat{\theta}} \right] \end{aligned}$$

Under the assumption that the prediction error $e_i(\hat{\theta}) = z_i - y_i(\hat{\theta})$ is uncorrelated,

$$\begin{aligned} F &= \sum_{i=0}^{N-1} \frac{dy_i(\hat{\theta})^T}{d\hat{\theta}} S_i^{-1} E\left[ e_i^T(\hat{\theta}) e_i(\hat{\theta}) \right] S_i^{-1} \frac{dy_i(\hat{\theta})}{d\hat{\theta}} \\ &= \sum_{i=0}^{N-1} \frac{dy_i(\hat{\theta})^T}{d\hat{\theta}} S_i^{-1} S_i S_i^{-1} \frac{dy_i(\hat{\theta})}{d\hat{\theta}} \\ &= \sum_{i=0}^{N-1} \frac{dy_i(\hat{\theta})^T}{d\hat{\theta}} S_i^{-1} \frac{dy_i(\hat{\theta})}{d\hat{\theta}} \end{aligned}$$

The result follows by inverting the Fisher information matrix. □

| Par | Ex.-1 (Constant UFR) (all data set) $\hat{\theta}_1 \pm$ SD | 95% CI | diag$(F^{-1})$ | (0-60)min $\hat{\theta}_2 \pm$ SD | Ex.-2 (Multi-step-wise UFR) (all data set) $\hat{\theta}_1 \pm$ SD | 95% CI | diag$(F^{-1})$ | (0-90)min $\hat{\theta}_2 \pm$ SD |
|---|---|---|---|---|---|---|---|---|
| $V_p(0)$ | 4.46±5.2e-3 | [4.45, 4.47] | 2.7e-5 | 4.47±5.5e-3 | 3.27±0.46e-3 | [3.26, 3.28] | 2.1e-5 | 3.27±5.2e-3 |
| $V_i(0)$ | 18.81±0.15 | [18.5, 19.1] | 0.02 | 18.82±0.23 | 12.19±0.028 | [12.13,12.25] | 7.78e-4 | 12.191±0.12 |
| $V_{rbc}$ | $1.42 \pm 0.056$ | [1.31, 1.54] | 3.1e-3 | 1.43±0.08 | 1.49±0.029 | [1.44,1.56] | 8.7e-4 | 1.49±0.1 |
| $K_f$ | 1.5e-3±4e-4 | [0.7e-3, 2.4e-3] | 1.7e-7 | 1.5e-3±6e-4 | 2.2e-3±4.8e-4 | [1.3e-3, 3.2e-3] | 2.3e-7 | 2.2e-3±1.3e-3 |
| $d_1$ | $1.36 \pm 0.52$ | [0.34, 2.37] | 0.27 | 1.36±0.73 | 1.06±0.36 | [0.36, 1.77] | 0.13 | 1.1±0.94 |
| $d_2$ | 0.02±0.057 | [-0.09, 0.13] | 3.3e-3 | 0.02±0.08 | 7.9e-3±0.019 | [-0.029, 0.045] | 3.54e-4 | 7.9e-3±0.048 |

Table I

ESTIMATION RESULTS USING HD DATA, THE CONSTANT UFR PROFILE (EXAMPLE 1) AND MULTI-STEP-WISE UFR PROFILE (EXAMPLE 2).

### D. Parameter Initialization Sensitivity

The uncertainty and uniqueness of the optimal solution, $\hat{\theta}$, can be investigated using randomly sampling a set of initial parameters $\Theta_0$ (uniform distribution) within bounded intervals centered around nominal values of the parameters we estimate. We choose the boundaries of the intervals to exclude unrealistic parameter variations and include all possible solutions.

For model (1), we compute the upper and lower boundaries of the intervals of the parameters ($V_p(0)$, $V_i(0)$, $V_{rbc}(0)$, $K_f$, $d_1$, $d_2$) within plausible physiological ranges centered around the nominal values of the parameters in Table II, using ±50% of the nominal values, which yields the set of vectors $\Theta_0 = [4.5, 1.5] \times [16.5, 5.5] \times [3, 1] \times [0.0086, 0.0029] \times [0.015, 0.005] \times [2.19, 0.73]$. In this set, we use the nominal volumes, $V_p = 3$, $V_i = 11$, and $V_{rbc} = 2$ (L), used in [13].

The output of this computational method is a distribution of optimal solutions represented by a probability density, which allows to understand how informative, unique, and uncertain a given estimated parameter set is. Therefore, if the distribution of the solutions is narrow or wide, we can conclude that the estimation either does or does not depend highly on the given initial parameters $\Theta_0$.

## IV. HD DATA EXAMPLES

We examined the performance of the estimation approach using two retrospective HD data sets used in ESKD patients. Two conventional UFR profiles were used, including a constant UFR profile and a multi-step-wise UFR profile, which applies different removal rates. Each data set contained noisy HCT measurements (the noisy measurements came from the sensor) collected at each 20 sec using the Crit-line monitor. The HCT was filtered and resampled at $T_s = 1$ min. We apply the estimation algorithm to estimate $\theta$ defined in Section (II-B).

The estimation was validated and compared using all data set (HCT and UFR) and the first 0-60 min. The Fisher information matrix ($F(\hat{\theta})$) was computed using the UKF, as illustrated in Theorem 1. To define the uncertainty around each estimated parameter value, we imposed 95% Confidence Intervals (CIs) around each parameter by $\hat{\theta} \pm$ SD1.96 where SD $= \sqrt{\text{diag}(F^{-1}(\hat{\theta}))}$ (standard deviation).

Due to high nonlinearity in the model (1), an analytical solution was difficult to obtain. However, the 4th order Runge-Kutta (RK4) with an integration time step of 0.1s was used to integrate the model. MATLAB Release 2020a was used to implement the algorithm and produce all results and simulations. Through each consecutive interval $(i-1)T_s \leq t \leq iT_s$, the UFR was held as a piecewise constant.

During this interval, we integrated the nonlinear model (1) forward with $\hat{\theta}$ using UFR and linked with the UKF to reconstruct the unobserved extracellular fluid volume and blood volume and forecast HCT. The UKF utilized a current measured HCT to update the fluid volume, blood volume, and the forecasted HCT. This process was repeated for each measured value of HCT to produce personalized predictions.

### A. Example 1 (Constant UFR Profile)

The constant UFR profile, as shown in Fig 3 A, was to remove a fluid volume of 2 L within 203 min (3 hrs, 40min) and at the rate of 600 mL/hr. We run the algorithm using the nominal values $\theta_0 = [3, 11, 2, 0.0057, 0.01, 1.46]^T$ as an initial guess. The parameters were estimated using all data set and the first 0-60 min data segment. This data segment was used to train the model and estimate the parameters, while the rest was for validation. Table I contains the estimated parameters.

In Fig. 3 B, the HCT (red) was simulated from the model using the constant UFR and the estimated $\hat{\theta}_1$, from all data set, while the HCT (green) was simulated using 0-60 min ($\hat{\theta}_2$). A good agreement was obtained between the actual HCT (B, balck) and the simulated HCTs (red, green). Negligible errors were observed between the two simulated HCTs, which can also be confirmed by the estimated parameters listed in Table I, in Columns 2 and 5 ($\hat{\theta}_1$ versus $\hat{\theta}_2$).

The uncertainty around each estimated parameter was defined by 95% CIs as shown in Table I where the estimated variances were computed from diag$(F^{-1}(\hat{\theta})) =$ [2.7e-5, 0.02, 3.1e-3, 1.7e-7, 0.27, 3.3e-3]$^T$. In Table I, narrow CIs were obtained for $V_p(0)$, $V_i(0)$, $V_{rbc}$, and $K_f$, characterizing the capability of the approach of estimating these parameters precisely. However, the computed CIs of the hydrostatic pressure parameters ($d_1$, $d_2$) were widely spread due to those parameters' insensitivity to HCT. The calculated Fisher matrix (Theorem 1) evaluated the accuracy of the estimation against model uncertainty and the noise in the measured HCT.

In Fig. 3, under the constant UFR, a nearly linear reduction in both $V_p$ and $V_i$ (Fig. C, D) was observed. The decrease in $V_p$ was due to the constant ultrafiltration, while the reduction in $V_i$ was due to the vascular refilling (interstitial to plasma) to balance the ultrafiltration. The plasma volume was reduced from 4.46L to 3.77L, indicating that only 0.69 L was removed from the plasma compartment at the end of the HD section.

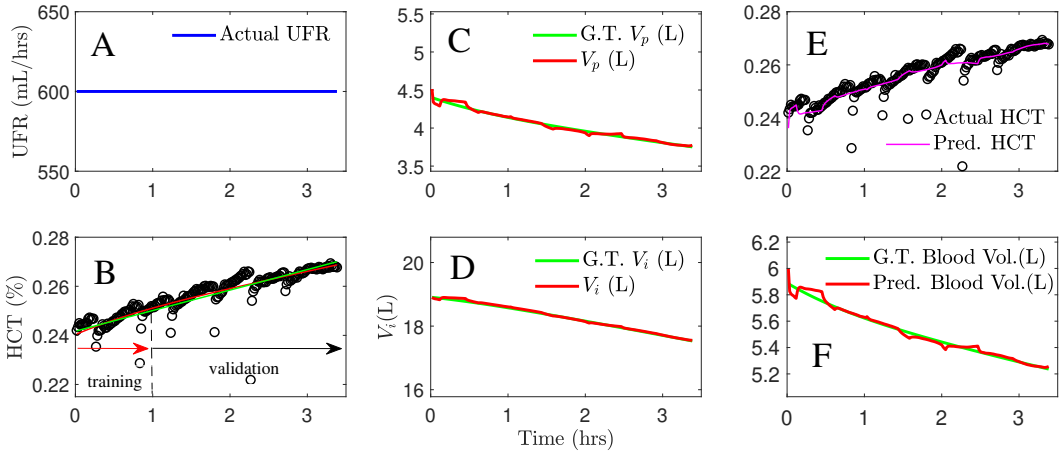


Figure 3. Estimation (A, B) using the constant UFR profile (A, blue) and actual HCT (B, black), simulated HCT (B, red) from all data set and simulated HCT (B, green) from (0-60min) for validation. Personalized predictions for the actual HCT using the UKF (E, magenta), and state estimations (C, D, F) for plasma volume (C, red), interstitial volume (D, red), and blood volume (F, red) using the UKF versus ground truth (GT) trajectories (green).

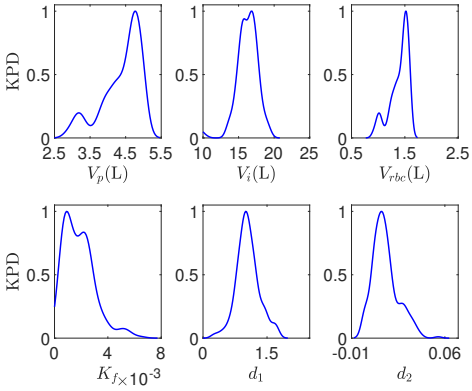


Figure 4. The Kernel Probability Density (KPD) estimate for the estimated parameters, for example-1, over the random initial solutions $\Theta_0$. The highest (peak) KPD parameter set is $\hat{\theta}_h = [4.7,\ 17.03,\ 1.5,\ 1e\text{-}3,\ 0.97,\ 0.012\ ]^T$.

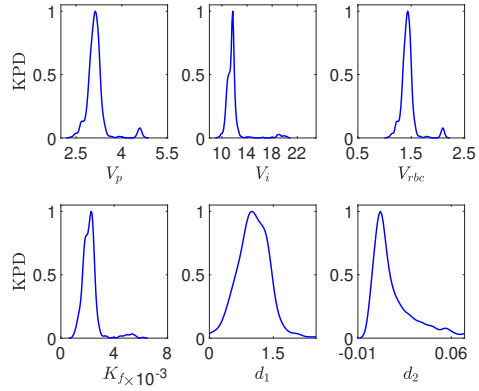


Figure 5. The Kernel Probability Density (KPD) estimate for the estimated parameters, for example-2, over the random initial solutions $\Theta_0$. The highest (peak) KPD parameter set is $\hat{\theta}_h = [3.13,\ 11.73,\ 1.44,\ 2.27e\text{-}3,\ 0.98,\ 6.9e\text{-}3\ ]^T$.

Since the target volume was 2L, thus 1.31L fluid volume was driven from the interstitial space to the plasma pool, during the fluid refilling process.

Personalized predictions for the actual HCT were obtained (Fig 3, E) using the UKF. These results show the ability of the method to predict the patient's outcomes during ultrafiltration when we implement the estimated parameters in the nonlinear model. Moreover, the method was able to reconstruct and correct the unobservable fluid and absolute blood volume (Fig 3, C, D, F) during ultrafiltration. These results were plotted along with ground truth (GT) trajectories calculated from the model (1) using $\hat{\theta}_1$ and the constant UFR profile.

The initial solution set $\Theta_0$ defined in Section (III-D) was used to generate a set of optimal solutions. In Fig .4, we showed the distribution of the solutions using the Kernel Probability Density (KPD) calculated by the function 'ks-density' in MATLAB. The KPD showed that the solution is virtually normally distributed around the set with the highest density (peak) $\hat{\theta}_h = [4.7,\ 17.03,\ 1.5,\ 1e\text{-}3,\ 0.97,\ 0.012\ ]^T$. This parameter set was close to $\hat{\theta}_1$, $\hat{\theta}_2$ (Table I) estimated using the nominal values $\theta_0$ as an initial guess.

### B. Example 2 (Multi-step-wise UFR Profile)

The HD prescription of the multi-step-wise UFR profile (Fig. 6, A) was to remove 3.86 L of excess fluid within 234 min (nearly 4hrs). Similarly, we used $\theta_0$ to estimate the parameters using all data set and a segment of data to validate the estimation. Because the UFR profile applied multiple step-rates, more data points (0-90min) were utilized by the model to capture the dynamics and estimate $\hat{\theta}$. In Table I, we listed the estimations with 95% CIs computed from the estimated variances $\text{diag}(F^{-1}(\hat{\theta})) = [2.1e\text{-}5,\ 7.78e\text{-}4,\ 8.7e\text{-}4,\ 2.3e\text{-}7,\ 0.13,\ 3.54e\text{-}4]^T$. As in example 1, the CIs were narrow except for the hydrostatic pressure parameters due to insensitivity to HCT. These results ensure the consistency of the estimation approach.

In Fig. 5, we showed the KPD for the optimal solutions estimated over the initial set $\Theta_0$. These solutions were nor-

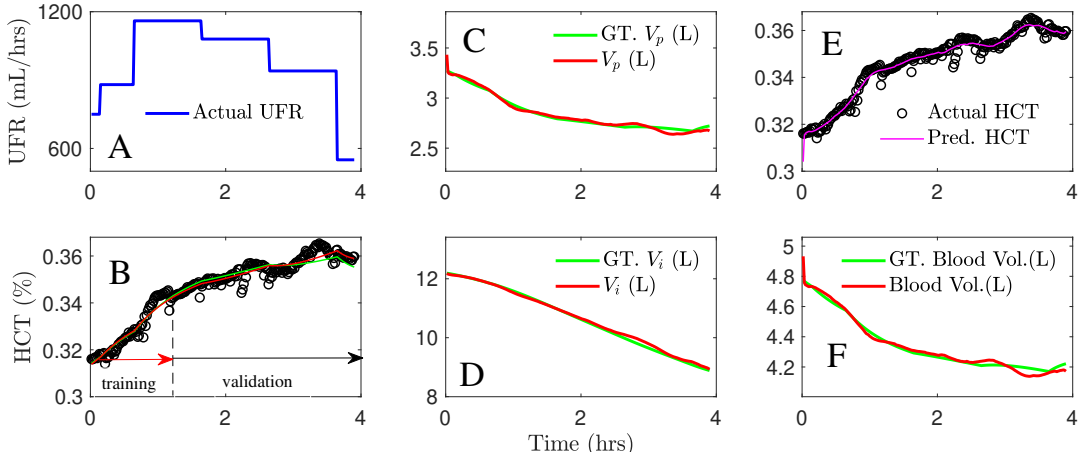


Figure 6. Estimation (A, B), for example-2, using the multi-step-wise UFR profile (A, blue) and actual HCT (B, black), and simulated HCT (B, red) from all data set and simulated HCT (B, green) from (0-90min) for validation. Personalized predictions for the actual HCT using the UKF (E, magenta), and state estimation (C, D, F) for plasma volume (C, red), interstitial volume (D, red), and blood volume (F, red) using the UKF versus ground truth (GT) trajectories (green).

mally distributed around the highest density solution (peak) at $\hat{\theta}_h = [3.13,\ 11.73,\ 1.44,\ 2.27\text{e-}3,\ 0.98,\ 6.9\text{e-}3\ ]^T$. Therefore, this set of parameters was close to $\hat{\theta}_1$, $\hat{\theta}_2$, (Table I, Column 6, 9) estimated using the nominal values in $\theta_0$.

As illustrated in Fig. 6, C, unlike the estimated reduction in plasma volume in example 1, here, the decrease in $V_p$ was roughly slight towards the end of the HD section, which is due to the decline in the removal rate applied by the ultrafiltration profile. As a result, the decrease in blood volume (F) was nearly balanced. This observation is crucial to prevent IDH events at the end of HD sections.

Personalized predictions for the actual HCT was obtained even though the UFR profile applied different removal steps during this treatment. The updated fluid and absolute blood volume were shown in Fig. 6 (C, D, F) with the GT trajectories generated from (1) using the estimated $\hat{\theta}_1$ and the step-wise UFR profile, while, the prediction of HCT was compared with the actual HCT (E, black). These results confirmed that the UKF was successfully able to correct and predict these variables under the multi-step-wise UFR profile.

## V. Discussion and Future Directions

We present a nonlinear model-based estimation framework to infer multiple physiological parameters and variables that have critical roles in fluid volume dynamics for people in ESKD, during ultrafiltration. However, ultrafiltration is not only the main goal of HD therapy. HD has other purposes, including a correction for acid-base derangements [3], [4], which utilize different types of physiological mathematical models. The accuracy of the estimation is calculated from the Fisher information matrix, demonstrated by the Theorem 1. We then apply this framework to clinical HD data consisting of standard and multi-step-wise UFR profiles and HCT measurements. These UFR profiles are used in HD treatments in a daily basis. To evaluate the estimation, we use all data sets and initial data segments for parameter estimation and validation.

We showed that the proposed approach provides good results, as demonstrated with numerical values (Table I) and simulations (Fig.3 and 6). However, due to the insensitivity of the hydrostatic capillary parameters to the HCT measurements, the CIs of these parameters are wide compared with the other parameters in both examples. We use the UKF to reconstruct blood and fluid (plasma, interstitial) volume and predict personalized HCT at each sampling time during ultrafiltration.

We explored the sensitivity of the estimation to initial solutions as a probability distribution. The distribution of the estimated solutions is kind of narrow and normally distributed around the solution with the highest KPD. Therefore, we concluded that the estimation does not depend highly on initial solutions and one good initial guess is to start with the nominal values.

In both examples, we showed by simulations (Fig.3, 6, C) that the estimated initial plasma volume was in an overload state ($V_p(0) > 3$L) [13]. Furthermore, with the constant UFR profile, we observed a rapid reduction in the blood volume before reaching the dry weight. This observation is commonly associated with the standard UFR because it uses high constant rates. However, the blood volume with the multi-step-wise UFR profile was slightly increased at the end of the session due to the decrease in the UFR rates. This observation clearly can be seen when we apply a personalized UFR, in which the UFR is objectively reduced as the time proceeds to the end of the session [13].

As future work, we will focus on clinical studies. We will apply this method to a large HD data set to obtain useful information for designing advanced HD treatments. Moreover, the proposed method could assist in diagnosing IDH events during the ultrafiltration process. The existing HD machines integrated sensors to monitor HCT and relative blood volume changes during the HD treatment. By incorporating the estimation method, we can predict the direction (reduction) in fluid volume and absolute blood volume ahead of time. We plan to incorporate this method into the existing HD

machine to predict IDH events, which has not been done yet. Finally, coupling this method with feedback-control systems to simultaneously estimate model parameters, update fluid and blood volumes, and predict IDH evens, during the treatment, is another future goal. In this feedback framework, blood volume is not only influenced by ultrafiltration but also by the patient's position or by taking a meal or drink during dialysis. We will implement external variables into the model to account for these circumstances. Since this feedback framework is our future goal, we did not discuss the potential implementation of the proposed method in this paper.

## VI. Conclusions

The primary goal of HD maintenance is to remove prescribed excess fluid and restore extracellular fluid volume to normal. Fluid overload and depletion are associated with high morbidity and mortality, including IDH. Therefore, knowledge of absolute blood volume and extracellular fluid in ESKD patients under HD treatment is critical to improving the outcomes.

This paper presents a new nonlinear estimation approach in the ESKD field to estimate the absolute blood volume, extracellular fluid volume, and underlying extracellular fluid shift/refill parameters and predict the change in the absolute blood volume during ultrafiltration. This method combines a nonlinear two-compartment fluid volume model whose critical parameters are estimated from patient data. The nonlinear least-squares method is used to estimate underlying model parameters and initial variables from patient's data, and linked with the UKF algorithm to bound error estimation, and update and predict fluid and absolute blood volume changes during the HD treatment. We derived results using clinical HD data examples that fluid and absolute blood volumes and the underlying model parameters can be estimated and bounded by the Fisher information matrix lower bounds. Furthermore, the method can reconstruct hidden fluid volume and provide personalized predictions for the change in the absolute blood volume (hematocrit) during ultrafiltration. The new estimation algorithm is now available to integrate into more advanced HD therapeutic machines and could improve HD treatment outcomes.

## Acknowledgements

The authors would like to thank Prof. Yossi Chait, University of Massachusetts Amherst, for his help and support.

## Appendix

### Appendix A:Fluid Volume Model

The equations for $P_c$ (hydrostatic capillary pressure), $P_i$ (interstitial pressure), $\pi_p$ (plasma colloid osmotic pressure), $\pi_i$ (interstitial colloid osmotic pressure) in (3b) are given by

$$P_c(t) = d_1\Big(100\frac{V_{rbc}+V_p(t)}{V_{rbc}+V_{p,eu}} + r\Big)^{d_2} + P_0 \tag{11a}$$

$$P_i(t) = \Big((100\frac{aV_i(t)}{V_{i,eu}}) + \frac{b}{(100\frac{aV_i(t)}{V_{i,eu}}+c)}\Big) \tag{11b}$$

$$\pi_p(t) = \Big(\frac{k_{c1}m_p}{V_p(t)} + \frac{k_{c2}m_p^2}{V_p^2(t)} + \frac{k_{c3}m_p^3}{V_p^3(t)}\Big) \tag{11c}$$

$$\pi_i(t) = \frac{k_{c1}m_i}{V_i(t)} + \frac{k_{c2}m_i^2}{V_i^2(t)} + \frac{k_{c3}m_i^3}{V_i^3(t)}\Big) \tag{11d}$$

where $V_{p,eu}$, $V_{i,eu}$ denote euhydration (normal) plasma and interstitial volume for 70 kg patient, respectively; $P_0$ is an offset pressure; $m_p$ is plasma protein mass; $m_i$ is interstitial protein mass, all are listed in Table II, in which $a$, $b$, $c$, $d_1$, $d_2$, $r$, $m_p$, $m_i$, $k_{c1}$, $k_{c2}$ and $k_{c3}$ are nominal parameters of model (1).

| Parameter | Value | Parameter | Value |
|---|---|---|---|
| $a$ | 0.006 | $K_f$ L/(min*mmHg) | 0.0057 |
| $b$ | -198 | $m_p$ (g) | 210 |
| $c$ | -45 | $m_i$ (g) | 210 |
| $d_1$ | 0.01 | $P_o$ (mmHg) | 13.128 |
| $r$ | -30 | $V_{i,eu}$ (L) | 11 |
| $d_2$ | 1.46 | $V_{p,eu}$ (L) | 3 |
| $g$ | 0.045 | $k_{c1}$ | 0.21 |
| $h$ | 0.7672 | $k_{c2}$ | 0.0016 |
| $l$ | 0.045 | $k_{c3}$ | 9e-6 |
| $V_{rbc}$(L) | 2 | - | - |

Table II
The nominal parameters of the nonlinear two-compartment model.

## References

[1] “"chronic kidney disease in the united state", us department of health and human services, centers for disease control and prevent, 2021. [online]. available: https://www.niddk.nih.gov/health-information/health-statistics/kidney-disease.”

[2] S. Ismael, M. Savalle, C. Trivin, F. Gillaizeau, C. DâAuzac, and C. Faisy, “The consequences of sudden fluid shifts on body composition in critically ill patients,” *Critical care*, vol. 18, no. 2, pp. 1–10, 2014.

[3] S. Marano, M. Marano, and L. Pecchia, “Frontiers in hemodialysis part ii: Toward personalized and optimized therapy,” *Biomedical Signal Processing and Control*, vol. 61, p. 102029, 2020.

[4] S. Marano, M. Marano, and F. J. Gennari, “A new approach to bicarbonate addition during hemodialysis: Testing model predictions in a patient cohort,” *IEEE Access*, vol. 10, pp. 17 473–17 483, 2022.

[5] S. Thijssen, F. Kappel, and P. Kotanko, “Absolute blood volume in hemodialysis patients: why is it relevant, and how to measure it,” *Blood purification*, vol. 35, no. 1-3, pp. 63–71, 2013.

[6] J. E. Flythe, S. E. Kimmel, and S. M. Brunelli, “Rapid fluid removal during dialysis is associated with cardiovascular morbidity and mortality,” *Kidney international*, vol. 79, no. 2, pp. 250–257, 2011.

[7] M. M. Assimon, J. B. Wenger, L. Wang, and J. E. Flythe, “Ultrafiltration rate and mortality in maintenance hemodialysis patients,” *American Journal of Kidney Diseases*, vol. 68, no. 6, pp. 911–922, 2016.

[8] E. Movilli, P. Gaggia, R. Zubani, C. Camerini, V. Vizzardi, G. Parrinello, S. Savoldi, M. S. Fischer, F. Londrino, and G. Cancarini, “Association between high ultrafiltration rates and mortality in uraemic patients on regular haemodialysis. a 5-year prospective observational multicentre study,” *Nephrology Dialysis Transplantation*, vol. 22, no. 12, pp. 3547–3552, 2007.

[9] “"epidemiology of kidney disease in the united states", us dept. national institutes of health, national institute of diabetes and digestive and kidney disease, 2018 [online]. available: https://pharm.ucsf.edu/kidney/need/statistics.”

[10] J. T. Daugirdas, “Pathophysiology of dialysis hypotension: an update,” *American journal of kidney diseases*, vol. 38, no. 4, pp. S11–S17, 2001.

[11] C. Loutradis, P. A. Sarafidis, C. J. Ferro, and C. Zoccali, "Volume overload in hemodialysis: diagnosis, cardiovascular consequences, and management," *Nephrology Dialysis Transplantation*, 2020.

[12] E. Seibert, S. G. Müller, P. Fries, J. Pattmöller, O. Kuss, G. H. Heine, M. Girndt, G. Schneider, P. Kotanko, F. Zhu *et al.*, "Calf bioimpedance spectroscopy for determination of dry weight in hemodialysis patients: effects on hypertension and left ventricular hypertrophy," *Kidney and Blood Pressure Research*, vol. 37, no. 1, pp. 58–67, 2013.

[13] R. Abohtyra, Y. Chait, M. J. Germain, C. V. Hollot, and J. Horowitz, "Individualization of ultrafiltration in hemodialysis," *IEEE Transactions on Biomedical Engineering*, vol. 66, no. 8, pp. 2174–2181, 2019.

[14] R. Abohtyra, C. Hollot, M. G. Germain, Y. Chait, and J. Horowitz, "Personalized ultrafiltration profiles to minimize intradialytic hypotension in end-stage renal disease," in *2018 IEEE Conference on Decision and Control (CDC)*. IEEE, 2018, pp. 309–314.

[15] M. Hueso, A. Vellido, N. Montero, C. Barbieri, R. Ramos, M. Angoso, J. M. Cruzado, and A. Jonsson, "Artificial intelligence for the artificial kidney: Pointers to the future of a personalized hemodialysis therapy," *Kidney Diseases*, vol. 4, no. 1, pp. 1–9, 2018.

[16] R. Agarwal, "How can we prevent intradialytic hypotension?" *Current opinion in nephrology and hypertension*, vol. 21, no. 6, pp. 593–599, 2012.

[17] O. Iimura, K. Tabei, H. Nagashima, and Y. Asano, "A study on regulating factors of plasma refilling during hemodialysis," *Nephron*, vol. 74, no. 1, pp. 19–25, 1996.

[18] A. C. Guyton and J. Hall, "The body fluid compartments: extracellular and intracellular fluids; interstitial fluid and edema," *Textbook of medical physiology*, vol. 11, p. 293, 2000.

[19] J. P. Kooman and F. M. van der Sande, "Body fluids in end-stage renal disease: statics and dynamics," *Blood Purification*, vol. 47, no. 1-3, pp. 223–229, 2019.

[20] S. Fleming, J. Wilkinson, C. Aldridge, R. Greenwood, S. Muggleston, L. Baker, and W. Cattell, "Dialysis-induced change in erythrocyte volume: effect on change in blood volume calculated from packed cell volume." *Clinical nephrology*, vol. 29, no. 2, pp. 63–68, 1988.

[21] L. Pstras, J. Waniewski, A. Wojcik-Zaluska, and W. Zaluska, "Relative blood volume changes during haemodialysis estimated from haemoconcentration markers," *Scientific Reports*, vol. 10, no. 1, pp. 1–9, 2020.

[22] C. Veillon, K. Y. Patterson, D. A. Nagey, and A. M. Tehan, "Measurement of blood volume with an enriched stable isotope of chromium (53cr) and isotope dilution by combined gas chromatography-mass spectrometry," *Clinical chemistry*, vol. 40, no. 1, pp. 71–73, 1994.

[23] D. Schneditz, J. Roob, M. Oswald, H. Pogglitsch, M. Moser, T. Kenner, and U. Binswanger, "Nature and rate of vascular refilling during hemodialysis and ultrafiltration," *Kidney international*, vol. 42, no. 6, pp. 1425–1433, 1992.

[24] R. M. Lindsay, T. Shulman, S. Prakash, G. Nesrallah, and M. Kiaii, "Hemodynamic and volume changes during hemodialysis," *Hemodialysis International*, vol. 7, no. 3, pp. 204–208, 2003.

[25] F. Zhu, D. Schneditz, E. Wang, K. Martin, A. Morris, and N. Levin, "Validation of changes in extracellular volume measured during hemodialysis using a segmental bioimpedance technique." *ASAIO journal (American Society for Artificial Internal Organs: 1992)*, vol. 44, no. 5, pp. M541–5, 1998.

[26] K. Kalantari, J. N. Chang, C. Ronco, and M. H. Rosner, "Assessment of intravascular volume status and volume responsiveness in critically ill patients," *Kidney international*, vol. 83, no. 6, pp. 1017–1028, 2013.

[27] Y. Dou, F. Zhu, and P. Kotanko, "Assessment of extracellular fluid volume and fluid status in hemodialysis patients: current status and technical advances," in *Seminars in dialysis*, vol. 25, no. 4. Wiley Online Library, 2012, pp. 377–387.

[28] A. D. Sinha, R. P. Light, and R. Agarwal, "Relative plasma volume monitoring during hemodialysis aids the assessment of dry weight," *Hypertension*, vol. 55, no. 2, pp. 305–311, 2010.

[29] A. Miller and J. Mandeville, "Predicting and measuring fluid responsiveness with echocardiography," *Echo research and practice*, vol. 3, no. 2, pp. G1–G12, 2016.

[30] Y. Ando, S. Yanagiba, and Y. Asano, "The inferior vena cava diameter as a marker of dry weight in chronic hemodialyzed patients," *Artificial organs*, vol. 19, no. 12, pp. 1237–1242, 1995.

[31] H. R. Kim, H. J. Bae, J. W. Jeon, Y. R. Ham, K. R. Na, K. W. Lee, Y. K. Hyon, and D. E. Choi, "A novel approach to dry weight adjustments for dialysis patients using machine learning," *Plos one*, vol. 16, no. 4, p. e0250467, 2021.

[32] K. Levenberg, "A method for the solution of certain non-linear problems in least squares," *Quarterly of applied mathematics*, vol. 2, no. 2, pp. 164–168, 1944.

[33] S. J. Julier and J. K. Uhlmann, "Unscented filtering and nonlinear estimation," *Proceedings of the IEEE*, vol. 92, no. 3, pp. 401–422, 2004.

[34] H. L. Van Trees, *Detection, estimation, and modulation theory, part I: detection, estimation, and linear modulation theory*. John Wiley & Sons, 2004.